*Research Article*

# Use of Silica Fume, Bentonite, and Waste Tire Rubber as Impermeable Layer Construction Materials

**Ahmet Şenol** [1] **and Arzu Guner** [2]

¹Cumhuriyet University, Faculty of Engineering, Civil Engineering Department, Sivas 58140, Turkey
²İzmir Metropolitan Municipality, İzbeton A. Ş, Bornova, İzmir, Turkey

Correspondence should be addressed to Ahmet Şenol; senol@cumhuriyet.edu.tr

To avoid the potential risks associated with all hazardous wastes, it is important that containment methods are intended to prevent the migration of liquid hazardous wastes or leaks containing hazardous components. Therefore, impermeable barriers were used to prevent contamination. In this study, geotechnical tests were performed on samples by mixing rubber and bentonite with silica fume at certain percentages. The aim of the experimental studies is to evaluate the applicability of certain proportions of silica fume, rubber, and bentonite mixtures as impermeable liner material. Possible cracks in bentonite during drying are reduced by the use of silica fume. Absorption of dynamic effects that may occur on the impermeable barrier layer is achieved by adding waste rubber in a uniform size. Several geotechnical tests were performed to examine the mixed rubber and bentonite with silica fumes. Looking at the results of the whole that mixed rubber and bentonite with silica fume yielded usable results and a blend for construction of a liner.

## 1. Introduction

Silica fume is a very fine noncrystalline $SiO_2$. It is collected as a by-product in factories that produce silicon and ferro-silicon alloy, which are captured by electrostatic filters. It is an ultrafine powder. The average particle diameter is 0.15 $\mu$m [1]. It is made at a temperature of approximately 1750°C–2000°C. Therefore, if spherical particles having a small diameter of nanoscale are released directly into the environment, the ambient particulate matter in the medium will be heavier (PM) [2].

The $SiO_2$ content is one of the main factors affecting the performance of silica fume and helps in pozzolanic activities. It can be used as an additive with silica fume in 88–92% $SiO_2$ and as an effective pozzolanic binding agent in concrete. When the concrete prepared with Portland cement and silica fume was tested, it was determined that there were increases in strength, pressure, and durability [3]. $SiO_2$ content of silica fume determines the usability of refractory castable materials as additives and as a raw material for the synthesis of SiC powder [4] and cordierite-mullite [5]. In addition, silica fume with a $SiO_2$ content <88% is very low in adhesion and their use is greatly reduced and is disposed of as solid waste, which presents health problems and atmospheric hazard. The increase in the amount of waste day by day means that the problems also increase, so it must be disposed of. In order to use it with higher efficiency, it is desirable to explore applicable areas.

Silica fume can be considered as a highly effective pozzolanic substance by incorporating the amorphous silica and the width of the surface area.

When silica fume was added to the mix to produce high performance concrete, and as a result of this mix, it showed a complex effect on compressive strength, depending on the silica calcium aluminate cement (CAC) content. Compressive strength increased when silica fume dosage was 20%. They found that when the silica fume is reduced by 10%, it affects the compressive strength negatively. They added steel fibers to the mixture, and this had a positive effect on the strength [6, 7]. Mixtures of silica fume and fly

ash may be used instead of Portland cement, which has various benefits in terms of strength and durability [8–10]. Microsilica reacts with $Ca(OH)_2$, and as a result, produces the C-S-H (gel) phase, so it is an active ingredient. During hydration, capillary porosity is reduced by the addition of silica fume, which can alter the microstructure of hydrated cakes due to the compact formation of C, S, H [11–13].

In recent years, a mixture of silica fume and bentonite has been used many times in the production of high strength concrete and stabilization of swelling clays, as a result of these studies, high values have been obtained in the strength of concrete and the swelling of the soil has been significantly improved [14, 15].

Magnesium ammonium phosphate cement (MAPC) with added silica fume and fly ash increased the late wet strength and reduced shrinkage due to drying. Therefore, it was concluded that the addition of spherical silica fume and fly ash to MAPC makes it more suitable for application in crack repair engineering [16].

Generally, sand and bentonite mixtures have been used to create impermeable barriers. Because of its ability to absorb leachate and low permeability, bentonite prevents polluted waters from reaching groundwater [17]. However, during barrier construction, shrinkage cracks may occur due to drying, which causes an increase in permeability folds.

When the mixtures prepared with bentonite are exposed to too much drying, it causes cracks, on the contrary, when it is exposed to too much wetting, it causes swelling. In order to eliminate these possible problems in the primer layer, bentonite is treated with cohesionless sand. Fly ash and similar binding materials have been discovered as a suitable additive in landfill lining [18].

In addition, some researchers have used fiber to improve performance and reduce cracks from shrinkage of clay. The specimens reinforced with fibers exhibited improved cracking resistance than unreinforced clay specimens. Studies on this subject can be used to study the behavior of clay barriers of critical geotechnical structures, particularly landfill cover exposed to drying cracking [19].

However, they stated that the total cost of the barrier could increase significantly due to the increase in the cost of using fiber [20]. The waste tire chip was proposed instead of fiber because of its low cost and easy availability. It has been determined that when 20% and 30% tire chips are used on silt-clay mixed soils, there is an increase in shear strength and cohesion, and a decrease in the internal friction angle. They concluded that the maximum strength of the compressed clay-rubber composite mixture gives values close to the maximum strength of the clay, and sometimes it may be better than it [21].

The usefulness of the liner system may be endangered if the liner material's strength is insufficient. To address this issue, the compacted sand-bentonite barrier can be modified by incorporating with waste tire fiber [22].

With the addition of granular waste rubber pieces to the black cotton soil, it was stated that the compressive strength increased and the swelling pressure decreased according to the triaxial test results [23]. It has been observed that the addition of cement and rubber chips causes an increase in the strength value without joints [24]. After mixing 5%, 10%, and 15% by the weight of pulverized rubber into kaolinite clay, they performed an undrained and drained triaxial test, resulting in 10% crumb. It has been stated that the maximum shear stress of rubber mixtures is less in undrained ones [25].

We have conducted this study to investigate the use of silica fume in impermeable clay layer at the base of solid waste landfill facilities. When you look at the history of the impermeable layer works, they were mostly prepared with fly ash and fiber additives to benefit from their binding properties. Since there are many thermal power plants in the world, it is very reasonable that the researches made on fly ash, which is the waste of this facility, are excessive. There is no study on impermeable layers by utilizing silica fume, which has high binding properties such as fly ash. We aimed to reduce the hydraulic conductivity by using rubber and bentonite, and we also added silica fumes to the impermeable layer to improve the engineering properties. Today, especially in industrial waste storage facilities, providing impermeability has become mandatory and the use of impermeable lining materials has become the most important component. Since the water leaking from the wastes is extremely harmful, groundwater and soil must be protected. For this purpose, sealing layers in landfills, sealing layer for slope safety, and vertical barriers are constructed. Sealing systems in sanitary landfills have become a priority construction.

If geological barriers make it difficult to build landfills, artificial sealing layers should be made of compacted soils (containing a significant amount of clayey particles) or other materials [26].

Industries working in the field of reuse of waste rubbers have been confronted with the problem of where to use this product. The United States annually generates about 279 million new waste tires, 85% of which are stored in storage areas, while the rest are illegally abandoned. The most useful way to reduce the ecological risks caused by scrap tires is not to accumulate or reuse. Today, waste rubber material is frequently used in playgrounds, bicycle paths, jogging tracks, stadiums, and road pavement layers [27].

One of the most effective ways of eliminating economic and environmental problems is through reprocessing. Waste rubber is transformed into different sizes and shapes as reinforcement material in construction, as a safety barrier on the edges of racetracks, and as a buffer in the hulls of vessels and vessels in berths due to its light weight, flexibility, energy absorption, sound, and heat insulation properties. Environmental regulations in developed countries require the use of barriers with very low permeability to protect against contamination caused by hazardous and chemical waste. Geosynthetic clay liners, clay, consolidated clay or bentonite-binding material mixtures and synthetic linings are widely used to prevent the spread of toxic and hazardous substances in waste landfill fields, water ponds, and storage areas. However, the use of geosynthetic clay coverings can be extremely expensive due to lack of suitable materials with high impermeability close to the disposal site or high costs of impermeable industrial liners. In similar situations, silica fume or silica fume stabilized soils would be beneficial to

industries that have to dispose of their waste safely. The industry can use it alone or in combination with other primers, if possible. A liner material must first have a very little permeability (less than 109 m/s). In addition, it must have sufficient mechanical behaviors such as high pressure, tensile strength, and flexibility [28].

## 2. Experimental Study

### 2.1. Materials

*2.1.1. Silica Fume.* The silica fume used for this study was a type ASTM C1240, which was obtained as waste product in the Ferro-Chromate factory in Turkey. After gathering through filters in the chimneys of arc furnaces, the silica fume was stored in closed bags so as not to react with the moisture in the atmosphere.

Chemical analysis of silica fume and results are presented in Table 1. Silica fume was used in different percentages with bentonite clay in the tests. Grain size distribution curve is plotted by mechanical analysis and hydrometer method (Figure 1). Specific gravity of silica fume by pycnometer method was obtained as GS = 2.22 according to ASTM D 854. The silica fume used was gray and was not plasticity. According to ASTM D-698, $w_{optimum} = 32.40\%$ and $\gamma_{dry} = 1.29 \, \text{Mg/m}^3$ were obtained using the standard proctor test.

Silica fume is very active and has very good pozzolanic properties. Silica fume is frequently used due to its usefulness in concrete [29, 30]. With the introduction of silica fume plasticizers, it has been used as an additive in concrete or as an additive in cement production in recent years [31–34].

For the reasons stated, it is considered the most valuable pozzolanic material. The X-ray diffraction (XRD) patterns of the bentonite and silica fume are given in Figure 2. When we look at the atomic distribution of bentonite in the unit cell, we see that it mostly contains 85% smectite, 5% calcite, 6% quartz, and 4% cristobalite. X-ray patterns (Figure 2) show that the silica fume particles used were essentially amorphous.

*2.1.2. Bentonite.* In Table 1, those found in the chemical structure of the bentonite used are shown in the max–min percentage range. In addition, the X-ray diffraction method was used to obtain the composition of the minerals that make up the bentonite used, and the results are given in Figure 2.

*2.1.3. Waste Rubber Tire.* The most uniform size of waste rubber tires (WRTs) was used in the test. WRT was stored in paper bags against the harmful effects of daylight. The gradation curve of the rubber is given in Figure 1.

*2.2. Methods.* The details of all the experiments performed are not detailed because many of them are known classical experiments. The experimental test program and the applied method are given in Table 2.

TABLE 1: The chemical compositions of bentonite and silica fume.

| Constituent (%) | Silica fume | Bentonite |
| --- | --- | --- |
| $SiO_2$ | 85–95 | 61.28–69.48 |
| $Fe_2O_3$ | 0.5–1.0 | 3.01–10.11 |
| $Al_2O_3$ | 1–3 | 13.18–17.79 |
| CaO | 0.8–1.2 | 4.54 |
| MgO | 1–2 | 2.10 |
| $Na_2O$ | 0.1–0.3 | 2.70 |
| $K_2O$ | 1.0–1.2 | 1.24 |
| $SO_3$ | — | 0.33 |
| $P_2O_5$ | — | <0.05 |
| S | 0.1–0.3 | — |
| C | 0.5–1.0 | — |
| Heat loss | 0.5–1.0 | — |
| $TiO_2$ | — | 1.11 |
| Loss on ignition | — | 1.10 |

*2.2.1. Mixture Design.* Rubber and bentonite were added to the silica fume by weight percent of the total mixture. The ratio of the total mixture by weight to silica is the highest. Because silica fume is considered as waste material to be recycled and it is binding. The amount of bentonite and rubber in the mixture was determined according to the dry weight of the mixtures. The percentages were selected as 0, 1, 3, 5, 7, 9, and 10%. Laboratory tests were performed according to the determined percentages. Table 3 shows the ratios of the mixture.

*2.2.2. Granulometry (Grain Size Distribution).* The grain size distributions of each mixture are determined separately and shown in Figure 1. Hydrometer analysis was performed for the amount of sample passing through the 200 sieve and the retained part was used for grain size distribution analysis.

*2.2.3. Specific Gravity.* The ASTM D-854 method guided us, and using this method, specific gravity values for all mixtures were determined experimentally. The conclusions are given in Table 4. While tests were performed, difficulties were observed in mixtures containing relatively high amounts of rubber (7, 9, and 10%). With air drawn from the pycnometer, low-density rubber deposited on the water, but to solve this problem, the rubber was kept under water by using a flexible chrome filter.

*2.2.4. Atterberg Limits.* Under the guidance of ASTM D 4318-84 method, no plasticity was observed in any of the samples.

*2.2.5. Hydraulic Conductivity.* To determine the coefficient of permeability of the samples using falling head method, the soil sample was placed in a tube and a flow through the sample was allowed. Coefficient of permeability for a falling head test is calculated using the following equation:

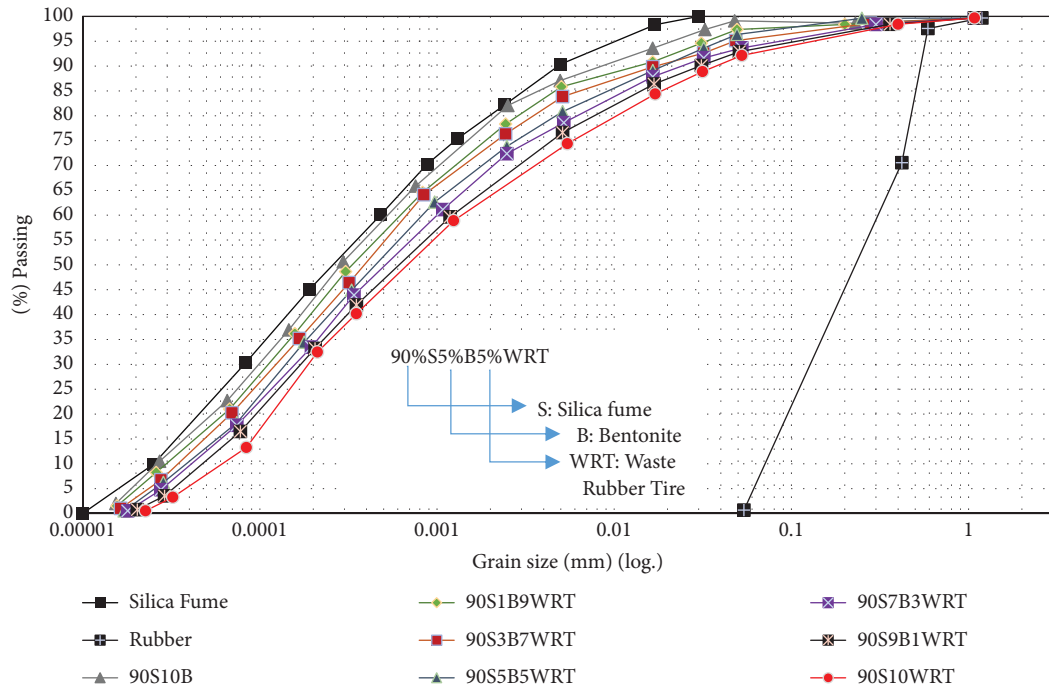$$K = 2.303 \frac{a \cdot L}{A \cdot t} \log \frac{h_1}{h_2}, \tag{1}$$
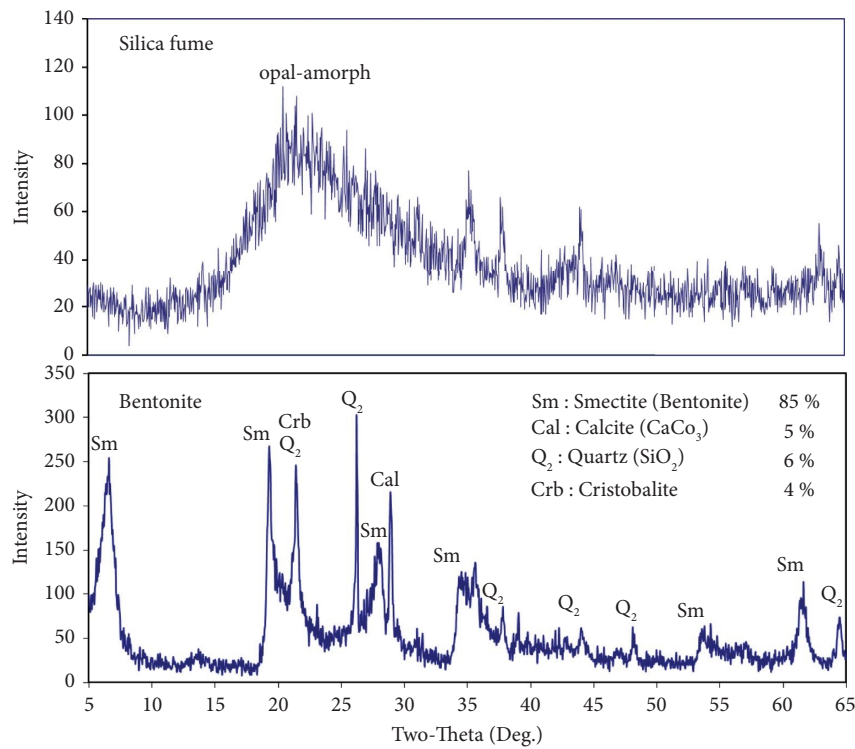
FIGURE 1: Grain size distribution curves.



FIGURE 2: XRD patterns of the bentonite and silica fume.

where $h$ represents the head difference at any time $t$, (the initial head difference, $h_1$, at time $t = 0$ is recorded, and water is allowed to flow through the soil such that the final head difference at time $t = t$ is $h_2$), $A$ represents cross-sectional area of specimen, $a$ represents the area of standpipe, and $L$ represents length of specimen.

TABLE 2: Experimental test program.

| Test performed | Method | Number of specimen | Dimensions of samples |
|---|---|---|---|
| Specific gravity | ASTM D-854 | 4 times | — |
| Consistency limits | ASTM D 4318-84 | 4 times | — |
| Hydraulic conductivity* | ASTM D5084 | 2 samples for each mixture | $H = 116$ mm, $D = 101.70$ mm |
| Compaction characteristics | ASTM D 698 | 4 samples for each mixture | $H = 105$ mm, $D = 115$ mm |
| Free swelling tests* | ASTM D-4546 | 4 samples for each mixture | $H = 20$ mm, $D = 50$ mm |
| Unconfined compressive strength* | ASTM D 2166 | 15 samples for each mixture | $H = 72$ mm, $D = 36$ mm |
| Split tensile strength* | ASTM C-496 | 15 samples for each mixture | $H = 76$ mm, $D = 38$ mm |
| Ultrasonic pulse velocity* | ASTM C 597 | 5 samples for each mixture | $H = 72$ mm, $D = 36$ mm |
| California bearing ratio (CBR) test* | ASTM D1883-05 | 4 samples for each mixture | $H = 177.8$ mm, $D = 152.5$ mm |

*All the specimens have been prepared according to compaction characteristics.

TABLE 3: Mixture design of the materials.

| Mixture no. | Abbreviation (sample ID) | Material type (% by weight) | | |
|---|---|---|---|---|
| | | Silica fume (S) | Bentonite (B) | Waste rubber tire (WRT) |
| 1 | 90S10B | 90 | 10 | 0 |
| 2 | 90S9B1WRT | 90 | 9 | 1 |
| 3 | 90S7B3WRT | 90 | 7 | 3 |
| 4 | 90S5B5WRT | 90 | 5 | 5 |
| 5 | 90S3B7WRT | 90 | 3 | 7 |
| 6 | 90S1B9WRT | 90 | 1 | 9 |
| 7 | 90S10WRT | 90 | 0 | 10 |

S: silica fume; B: bentonite; WRT: waste rubber tire.

TABLE 4: Physical characteristics of the mixtures.

| Sample ID | Specific gravity | Maximum dry density $(\gamma_{dry}, \text{Mg/m}^3)$ | Optimum water content ($W_{optimum}$, %) |
|---|---|---|---|
| 90S10B | 2.39 | 1,329 | 31 |
| 90S9B1WRT | 2.27 | 1,311 | 31.2 |
| 90S7B3WRT | 2.08 | 1,303 | 31.4 |
| 90S5B5WRT | 1.72 | 1.29 | 31.6 |
| 90S3B7WRT | 1.97 | 1,289 | 31.2 |
| 90S1B9WRT | 2.02 | 1,286 | 30.6 |
| 90S10WRT | 2.31 | 1,284 | 29.5 |

The permeability test tube had a stainless steel plate. The mixtures were cured for 7 or 28 days. After curing, permeability test was applied. The hydraulic conductivity $K$ values of the samples were calculated using equation (1). Permeability tests were performed on three similar samples.

### 2.2.6. Unconfined Compressive Strength.

Unconfined compression (UC) tests were performed on samples cured after compression. Deformation controlled load application was performed. The curing time for all samples was 7 and 28 days.

The samples were compacted into a steel mold with diameters and heights of 36 mm and 72 mm, respectively, and then extracted for testing. All samples were subjected to a strain deformation of 0.5 mm per minute. Tests were performed on five samples with the same characteristics. The test results were evaluated by taking into consideration the means of near-close values.

### 2.2.7. Splitting Tensile Strength.

Specimens were prepared for splitting test with static compaction tool and all cured and compacted samples were tested. The plates of the compression testing machine are placed above and below the cylindrical sample. In accordance with ASTM C-496, the test was performed on all samples. All samples were subjected to a strain deformation of 0.5 mm per minute for the splitting tensile strength tests. The sample is loaded until splitting in the vertical direction occurs. According to the results of the tests, splitting tensile strength was calculated using the following equation:

$$f_{st} = \frac{2P}{\pi \cdot L \cdot D} \Big\}, $$

$P$: the maximum load on the specimen $(N)$,

$D$: the di ameter of the specimen $(mm)$,

$L$: the length of the specimen $(mm)$,

(2)

where $f_{st}$ is the splitting tensile strength (MPa). At least three samples were tested for each mixture. Averages and standard deviation from the obtained data were analyzed [35].

*2.2.8. Sample Preparation.* The materials used in the mixture were air-dried in the drying room in the laboratory environment. All mixtures were mixed at the optimum water percentage. Then, the mixtures were kept at $25 \pm 2°C$ and $64 \pm 5\%$ humidity in the laboratory environment to keep the moisture content in the dry mix constant. Samples with a diameter of 38 mm and a length of 76 mm were prepared from the mixtures, statically compressed by simple compression method and wrapped with elastic film. An automatic compactor device was used to ensure the standard in the compression of the samples. Compressed samples were kept for three different curing, 7, 14, and 28 days. The prepared samples were covered with a waterproof barrier during the curing process and kept in the environmental chamber at $20 \pm 2°C$ and $100 \pm 5\%$ humidity for the moisture-controlled curing.

## 3. Experimental Results and Discussion

*3.1. Grain Size Distribution.* Particle size analyzes were performed on the mixtures. Hydrometer analysis was applied by taking some of the soil, which was washed and passed through sieve no. 200. As can be seen from the distribution curves, the distribution curve shifted towards the coarser region with the increase in the rubber percentage in the mixture.

*3.2. Specific Gravity.* The specific gravity results data, according to Table 4, show that when the percentage of bentonite and the percentage of rubber increases, GS value falls from 2.39 to 1.72 as expected. While testing, rubber floated on water due to low density and accumulated at the entrance of the pycnometer, the amount was neglected because it was so small.

*3.3. Compaction Characteristics.* The compaction characteristics of all results are given in Table 4. The maximum dry density decreases as the percentage of rubber in the mixtures increases. The percentage of rubber in the mixtures had an effect on the maximum dry density, one increasing and the other decreasing.

*3.4. Hydraulic Conductivity.* The coefficient of permeability results obtained according to the hydraulic conductivity results made on compressed and hardened samples for 28 days is shown in Figure 3. As can be seen from the graphs, a decrease in the percentage of bentonite caused a decrease in hydraulic conductivity and the percentage of waste rubber tire increased for both compacted and cured samples.

*3.5. Unconfined Compression Tests.* Curing period and unconfined compressive strength change curves are plotted in Figure 4. As observed from percentage of waste rubber tire
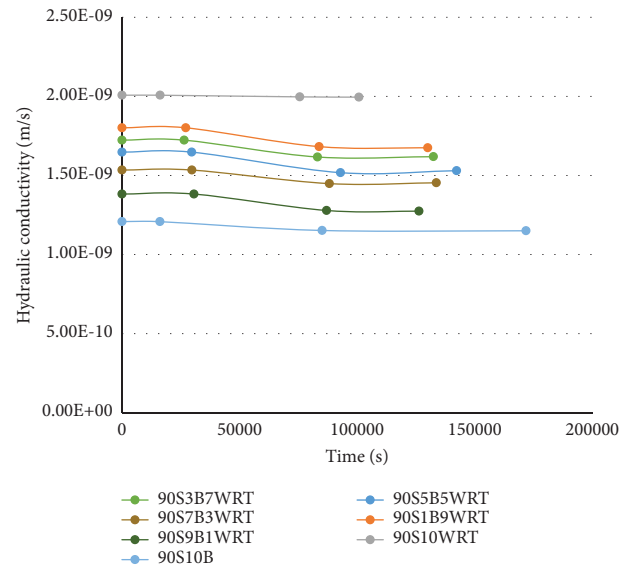


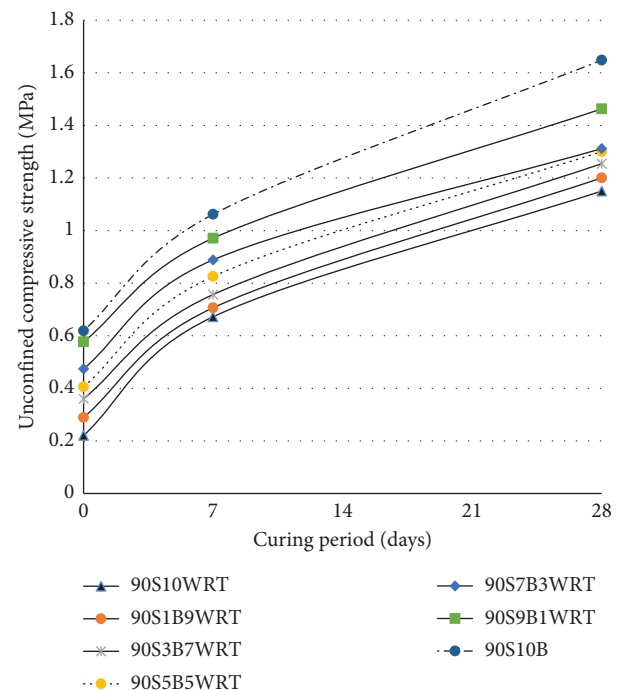FIGURE 3: Hydraulic conductivity from the falling head permeability test.



FIGURE 4: Unconfined compressive strength versus curing period.

and bentonite in Figure 4, one increases and the other decreases, UC strength increases.

According to the unconfined compressive strength, the increase in the percentage of waste rubber (0 to 10%) and the decrease in the percentage of bentonite (10 to 0%) caused the UC strength to increase up 2.8 times in the mixes. This increases were approximately 2.13 times for 7 days and 1.6 times for 28 days cured specimens. Figure 4 shows that the strength of the samples increases as the silica fume increases. In addition, secant Young's modulus increases as

curing periods increases. UC strengths at 7 days were decreased 3.05–1.68 times. The amount of rubber and bentonite affected the outcome of this situation. In the first 7 days, the fastest decline occurred and this decline continues at a much lower rate until the end of 28 days. Using stress–strain data, Young's module was calculated for each sample and recorded as secant Young's module ($E_{50}$) depending on the curing periods as given in Figure 5.

As the amount of rubber increased and the amount of bentonite decreased, the secant Young's modulus increased. This increase in secant Young's modulus is due to rubber tire. Compression tests have shown that the mixtures with high rubber content showed high strains during failure.

To estimate deformation (elasto-plastic) energy capacity behavior of mixing samples, the stress–strain curve of a 28-day cured sample is plotted in Figure 6. Taking into account (Figure 6), strain values of high strength at maximum stress shows that 3.48% is obtained for the sample without waste rubber tire and 4.24% for the sample with the highest amount of waste rubber tire (10%). Taking into account the areas under the stress-strain curves, the elastoplastic energy capacities are decreased and plastic energy capacities are increased with the reduction of waste rubber tire. Flexibility and elastic rubber mode change can be attributed to the decrease in elastic energy capacities. Thus, a flexible material is obtained with silica fume added with rubber.

### 3.6. Splitting Tensile Strength.

According to splitting tensile strength results, when Figure 7 is examined, the splitting tensile strength has decreased, which can be explained by the increases in the waste rubber tire percentage and the bentonite percentage decreases.

As can be seen from Figure 7, as the curing time increases, the tensile strength increases. The fastest increase was in the first 7 days and continued at a smaller rate until the 28-day curing time. As a result of the splitting test, as the percentage of rubber in the samples increased, the sample tended to remain in one piece. Cracks in some samples appeared early during the experiment. This depends on the amount of silica fume in the samples. Waste rubber tire particles acting as shock absorber delayed the expansion of existing cracks. Samples with high percent waste rubber tire showed a ductile type of failure, and the separation was longer. This can be explained by the fact that the rubber (waste rubber tire percent >5) increases the plastic energy capacity of the specimens. Therefore, the samples show a large ductile behavior before failure (showing up to 10% strains at failure).

### 3.7. California Bearing Ratio.

The results of CBR test shows the soaked and unsoaked CBR values of mixtures. The case of soaked condition has been carried out in this study. The variation in the average CBR values of all mixture is shown in Figure 8. It was concluded that adding additives have significant changes in C.B.R values. Adding bentonite only increased C.B.R value from 12.35% to 16.5% while adding rubber only slightly decreased CBR.
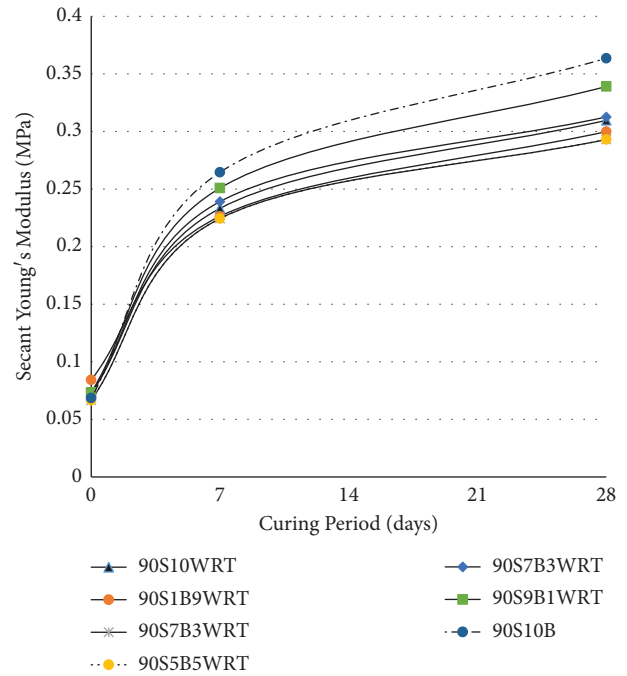


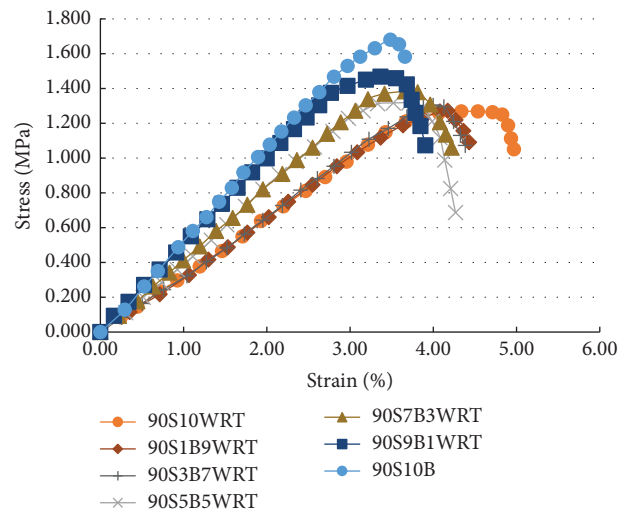Figure 5: Secant Young's modulus versus curing period.



Figure 6: Stress-strain diagram of 28 days cured specimens.

Compressed samples were soaked in water, so they swelled. Swelling percentages of compacted samples are shown in Figure 9 for curing periods of 28 days. It was found that the free swelling percentages dramatically increased by adding bentonite only to the mixtures. The bentonite content had an effect on the swelling capacity of the samples and terminated within 2–7 days. The following conclusion can be drawn from this graph. As a result of the increase in the rubber percentage and the decrease in the bentonite percentage, the swelling pressure decreases as expected.

### 3.8. Ultrasonic Velocity.

Another method of determining the effects of freeze-thaw on samples is ultrasonic velocity measurements. Three mixtures were prepared for this test.
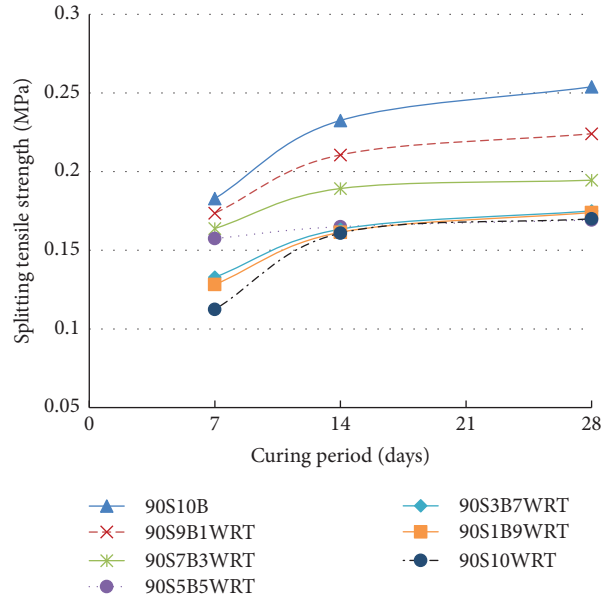
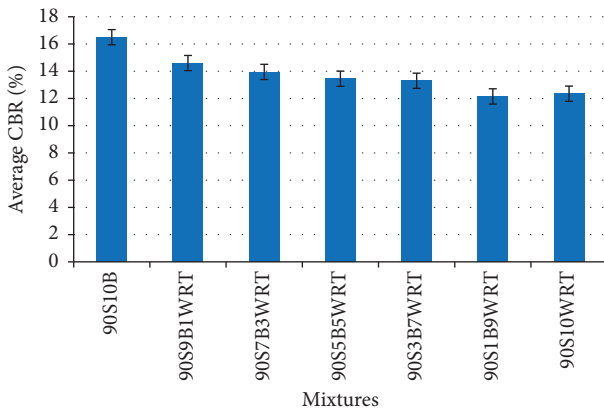Figure 7: Splitting tensile strength versus curing period.
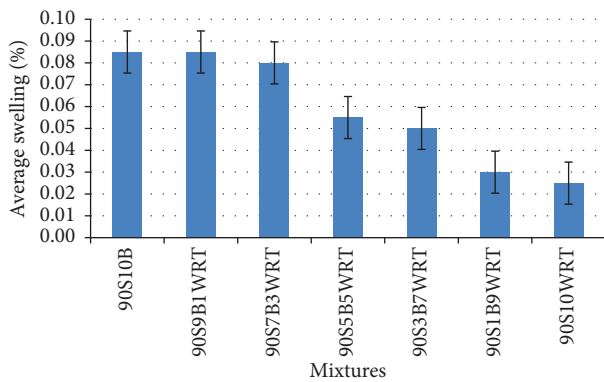


Figure 8: CBR values of all mixture.



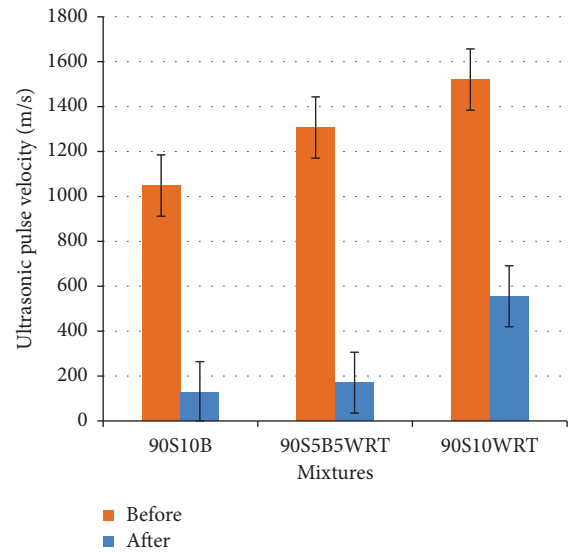Figure 9: The results of free swelling tests.



Figure 10: Ultrasonic pulse velocity versus freeze/thaw cycles.

7 days before testing and each mixture was tested before and after freezing/thawing cycles. The samples were placed in the freezer for 4 days and then placed in a humidity chamber for 3 days. The temperature of $-21°C \pm 1°C$ in the freezer was constant during the experiment. The humidity chamber temperature is 22°C and contains 95% humidity. At the end of the three cycles, no significant negativity was detected on the surface of the samples, but the ultrasonic pulse velocity values decreased significantly before and after the test. The test results are given in Figure 10.

The microfractures in the transition region of the samples and the increase in the volume of voids may explain the decrease in the freeze-thaw cycles; however, the stabilized sample capability will result in the decrease in ultrasonic transfer capability.

The first mixture contained the highest amount of bentonite, the second mixture contained the highest amount of waste rubber tire, and the third mixture contained 5% waste rubber tire and 5% bentonite. The tests were allowed to cure for
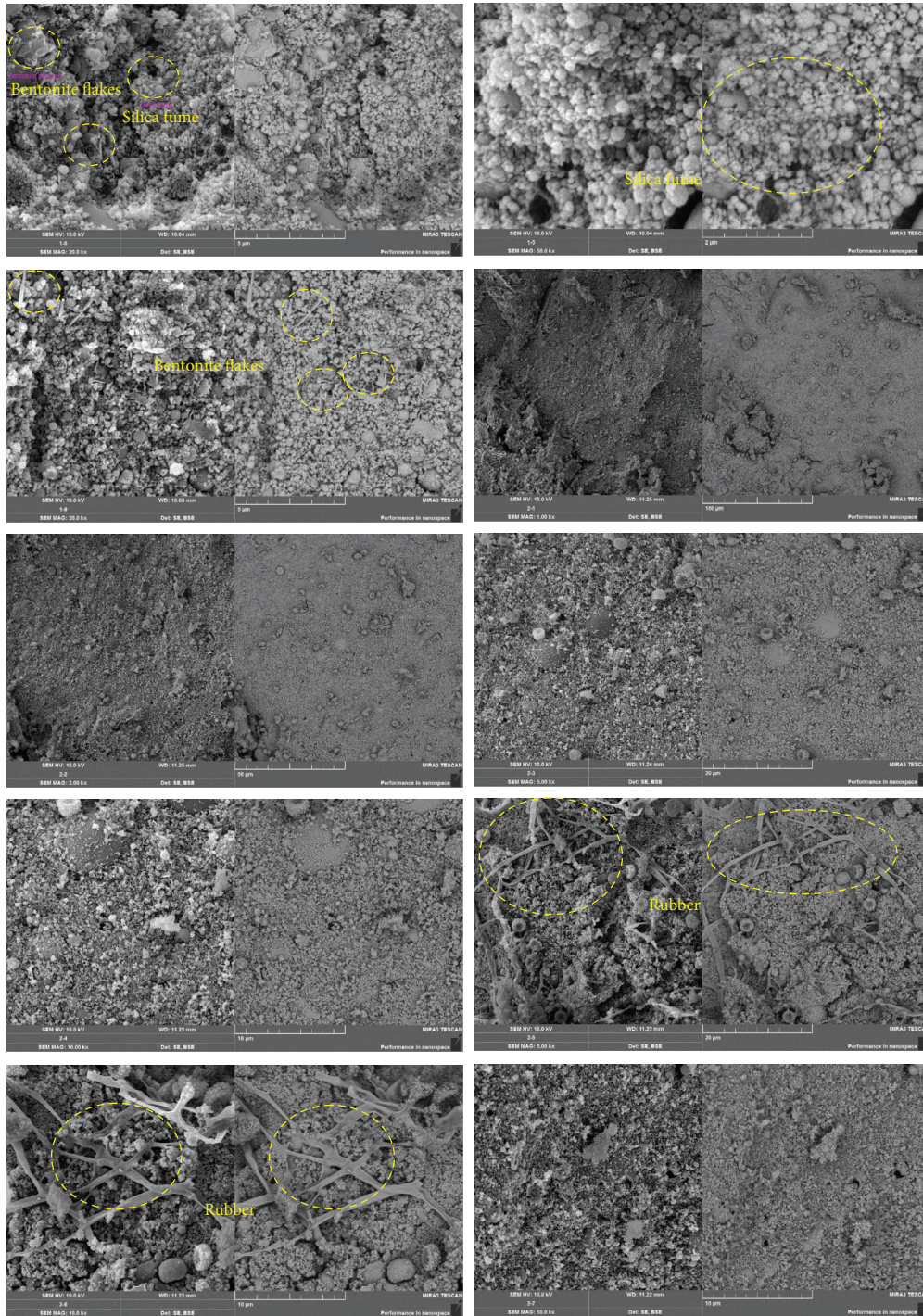
FIGURE 11: Microstructural analysis of samples with and without rubber added using SEM.

FE-SEM analysis is an ideal analysis to see the microstructural mechanisms. UCS and splitting tensile strength effect on waste rubber tire and bentonite can be seen by SEM analysis. In Figure 11, the microstructural arrangement of silica fume, bentonite, and rubber is clearly seen. Figure 11 shows the microstructure of samples with and without 10% rubber added at $2\,\mu$m–$100\,\mu$m. There are voids in the sample, which can be observed in the analysis. In addition, a very intense relationship can be observed between silica fume and bentonite. CSH gel fills the gap in the mixtures and indicates that a tight matrix is formed. Figure 12 shows the EDX analysis of the selected SEM images for 10% bentonite and 10% rubber content. Si peaks in all mixtures. The most important reason for this is thought to be due to the
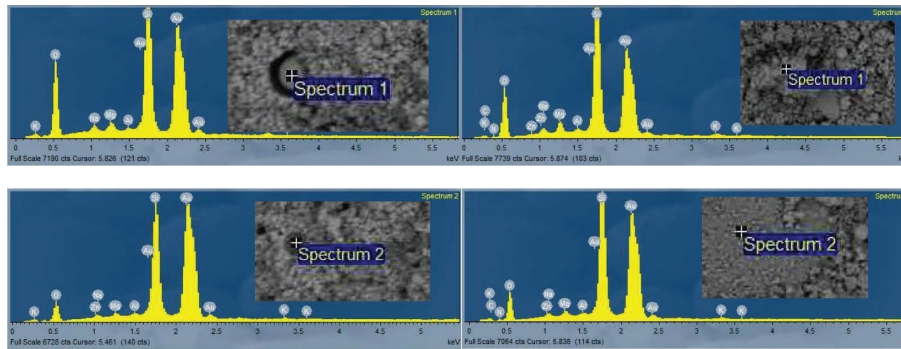
FIGURE 12: EDX spectra of samples with and without rubber added.

hydration reaction. However, the formation of the pozzolanic effect can also be understood from the high silica peak. This is mostly followed by alumina peaks.

## 4. Conclusions

Tests, which are frequently used in the geotechnical field, were carried out on samples formed with mixtures of rubber, bentonite, and silica fume. The usability and applicability of silica fume, rubber, and bentonite mixtures as insulation material in terms of hydraulic conductivity were evaluated. The following results were obtained from these experimental studies.

Both the increase of the percentage of rubber in the mixtures increased the hydraulic conductivity and the decrease of the percentage of bentonite increased the hydraulic conductivity. This was also seen in both compressed and cured samples.

In addition, the increase in the percentage of rubber caused a decrease in unconfined compressive strength.

Curing of specimens remaining in water for 7 and 28 days increases the unconfined compressive strength. During the first 7 days, there was a big change in the free pressure resistance, but after 28 days it decreased and approached a fixed value. The increase rate is very high in the first 7 days.

The increase in the percentage of rubber also led to a decrease in the secant Young's modulus. The ductile behavior of the samples increased with the addition of rubber and their elastic energy capacities decreased. If you use it as an impermeable layer under the solid waste landfill area, specimens have shown that, in a negative situation it can absorb more energy at the moment specimens resulted in a flexible material.

The increase in the amount of waste rubber tire caused a decrease in the splitting tensile strength. Curing of specimens increased splitting tensile strength. Furthermore, the increase in the percentage of waste rubber tire forced the samples to behave as a ductile material and the separation was gradual. In addition, this is extremely important to use it as a impervious liner material in many areas requiring insulation.

The increase in waste rubber tire percentage also increased compressibility. The curing period was effective in this case.

Free swelling increases as bentonite percent increases according to CBR test results.

The three freeze and thaw cycles did not have a noticeable effect on the sample surface but ultrasonic pulse velocity of the specimens decreased considerably after freeze/thaw cycles.

The most important value that can be extracted from the experiments in terms of hydraulic conductivity is provided by silica fume with up to 10% waste rubber tire and bentonite, which seems to be an optimum material for making an impervious liner. The desired flexibility in an impermeable liner is also achieved by the addition of waste rubber tire.

Experimental results have shown that waste rubber tire, bentonite, and silica fume can work together. In case these materials are used as land application, compaction and proportions should be taken into consideration. In addition, the elasticity properties of waste rubber tires should be reviewed against the effects of daylight degradation.

If this material is used for impermeable liner applications, you will evaluate large quantities of silica fume as well as the use of some amount of waste rubber, which has become a problem in the world. When you create silica fumes and similar industrial wastes in this way, it has the advantage of reusing the industrial waste by-product, which is less polluting the environment or minimizing negative effects on land uses.

## Data Availability

The experimental data used to support the findings of this study are available from the corresponding author upon request.

## Conflicts of Interest

The authors declare that they have no conflicts of interest.

## References

[1] N. Gaurina-Međimurec, K. Sedić, A. Čajić, A. Matijević, and A. Matijević, "Effect of microblock on the compressive strength of Portland cement at elevated temperatures," *Polar and Arctic Sciences and Technology; Petroleum Technology*, vol. 8, pp. 41–51, 2017.

[2] E. Chalvatzaki, V. Aleksandropoulou, T. Glytsos, and M. Lazaridis, "The effect of dust emissions from open storage piles to particle ambient concentration and human exposure," *Waste Management*, vol. 32, no. 12, pp. 2456–2468, 2012.

[3] M. Mazloom, A. A. Ramezanianpour, and J. J. Brooks, "Effect of silica fume on mechanical properties of high-strength concrete," *Cement and Concrete Composites*, vol. 26, no. 4, pp. 347–357, 2004.

[4] Y. Zhong, L. L. Shaw, M. Manjarres, and M. F. Zawrah, "Synthesis of silicon carbide nanopowder using silica fume," *Journal of the American Ceramic Society*, vol. 93, no. 10, pp. 3159–3167, 2010.

[5] R. M. Khattab, A. M. El-Rafei, and M. F. Zawrah, "In situ formation of sintered cordierite-mullitenano-micro composites by utilizing of waste silica fume," *Materials Research Bulletin*, vol. 47, no. 9, pp. 2662–2667, 2012.

[6] F. Wang, X. Sun, Z. Tao, and Z. Pan, "Effect of silica fume on compressive strength of ultra-high-performance concrete made of calcium aluminate cement/fly ash based geopolymer," *Journal of Building Engineering*, vol. 62, Article ID 105398, 2022.

[7] M. I. Khan and R. Siddique, "Utilization of silica fume in concrete: review of durability properties," *Resources, Conservation and Recycling*, vol. 57, pp. 30–35, 2011.

[8] S. A. Barbhuiya, J. K. Gbagbo, M. I. Russell, and P. A. M. Basheer, "Properties of fly ash concrete modified with hydrated lime and silica fume," *Construction and Building Materials*, vol. 23, no. 10, pp. 3233–3239, 2009.

[9] T. Nochaiya, W. Wongkeo, and A. Chaipanich, "Utilization of fly ash with silica fume and properties of Portland cement–fly ash–silica fume concrete," *Fuel*, vol. 89, no. 3, pp. 768–774, 2010.

[10] V. Lilkov, I. Rostovsky, O. Petrov, Y. Tzvetanova, and P. Savov, "Long term study of hardened cement pastes containing silica fume and fly ash," *Construction and Building Materials*, vol. 60, pp. 48–56, 2014.

[11] E. Sakai, S. Miyahara, S. Ohsawa, S. H. Lee, and M. Daimon, "Hydration of fly ash cement," *Cement and Concrete Research*, vol. 35, no. 6, pp. 1135–1140, 2005.

[12] Z. Giergiczny and A. Król, "Immobilization of heavy metals (Pb, Cu, Cr, Zn, Cd, Mn) in the mineral additions containing concrete composites," *Journal of Hazardous Materials*, vol. 160, no. 3, pp. 247–255, 2008.

[13] K. L. Lin, W. C. Chang, D. F. Lin, H. L. Luo, and M. C. Tsai, "Effects of nano-SiO2 and different ash particle sizes on sludge ash-cement mortar," *Journal of Environmental Management*, vol. 88, no. 4, pp. 708–714, 2008.

[14] M. Raza, K. Shahzad, A. Afridi, and M. Hasnain, "Effect of silica fume and bentonite on strength and durability of high performance concrete," *GSJ*, vol. 7, pp. 166–178, 2019, https://www.globalscientificjournal.com/researchpaper/Effect_of_Silica_fume_and_Bentonite_on_strength_and_durability_of_High_Performance_Concrete.pdf.

[15] E. Sheraz, "Effect of silica fume and bentonite on strength and durability of high performance concrete," *IJSTE - International Journal of Science Technology & Engineering*, vol. 5, no. 6, 2018, https://ijste.org/Article.php?manuscript=IJSTEV5I6014.

[16] D. Dong, Y. Huang, Y. Pei et al., "Effect of spherical silica fume and fly ash on the rheological property, fluidity, setting time, compressive strength, water resistance and drying shrinkage of magnesium ammonium phosphate cement," *Journal of Building Engineering*, vol. 63, Article ID 105484, 2023.

[17] K. Mukherjee and A. K. Mishra, "Hydraulic and mechanical characteristics of compacted sand–bentonite: tyre chips mix for its landfill application," *Environment, Development and Sustainability*, vol. 21, no. 3, pp. 1411–1428, 2019.

[18] C. B. Gupt, S. Bordoloi, R. K. Sahoo, and S. Sekharan, "Mechanical performance and micro-structure of bentonite-fly ash and bentonite-sand mixes for landfill liner application," *Journal of Cleaner Production*, vol. 292, Article ID 126033, 2021.

[19] U. Chaduvula, B. V. S. Viswanadham, and J. Kodikara, "Centrifuge model studies on desiccation cracking behaviour of fiber-reinforced expansive clay," *Geotextiles and Geomembranes*, vol. 50, no. 3, pp. 480–497, 2022.

[20] J. S. Yadav and S. K. Tiwari, "Effect of waste rubber fibres on the geotechnical properties of clay stabilized with cement," *Applied Clay Science*, vol. 149, pp. 97–110, 2017.

[21] Z. H. Özkul and G. Baykal, "Shear behavior of compacted rubber fiber-clay composite in drained and undrained loading," *Journal of Geotechnical and Geoenvironmental Engineering*, vol. 133, no. 7, pp. 767–781, 2007.

[22] K. Mukherjee and A. Kumar Mishra, "Recycled waste tire fiber as a sustainable reinforcement in compacted sand–bentonite mixture for landfill application," *Journal of Cleaner Production*, vol. 329, Article ID 129691, 2021.

[23] A. Srivastava, S. Pandey, and J. Rana, "Use of shredded tyre waste in improving the geotechnical properties of expansive black cotton soil," *Geomechanics and Geoengineering*, vol. 9, no. 4, pp. 303–311, 2014.

[24] L. Xin, J. He, H. Liu, and Y. Shen, "Potential of using cemented soil-tire chips mixture as construction fill, a laboratory study," *Journal of Coastal Research*, vol. 73, no. 1, pp. 564–571, 2015.

[25] M. Tajdini, A. Nabizadeh, H. Taherkhani, and H. Zartaj, "Effect of added waste rubber on the properties and failure mode of kaolinite clay," *International Journal of Civil Engineering*, vol. 15, no. 6, pp. 949–958, 2017.

[26] M. Wasil, "Effect of bentonite addition on the properties of fly ash as a material for landfill sealing layers," *Applied Sciences*, vol. 10, no. 4, p. 1488, 2020.

[27] A. Al-Tabbaa and T. Aravinthan, "Natural clay-shredded tire mixtures as landfill barrier materials," *Waste Management*, vol. 18, no. 1, pp. 9–16, 1998.

[28] E. Cokca and Z. Yilmaz, "Use of rubber and bentonite added fly ash as a liner materialfi y ash as a liner material," *Waste Management*, vol. 24, pp. 153–164, 2004.

[29] E. Kalkan and S. Akbulut, "The positive effects of silica fume on the permeability, swelling pressure and compressive strength of natural clay liners," *Engineering Geology*, vol. 73, no. 2, pp. 145–156, 2004.

[30] E. Kalkan, "Preparation of scrap tire rubber fiber–silica fume mixtures for modification of clayey soils," *Applied Clay Science*, vol. 81, pp. 117–125, 2013.

[31] G. Adil, J. T. Kevern, and D. Mann, "Influence of silica fume on mechanical and durability of pervious concrete," *Construction and Building Materials*, vol. 247, Article ID 118453, 2020.

[32] X. Wu, Y. Shen, and L. Hu, "Performance of geopolymer concrete activated by sodium silicate and silica fume activator," *Case Studies in Construction Materials*, vol. 17, p. 1513, 2022.

[33] M. Adamu, M. L. Marouf, Y. E. Ibrahim, O. S. Ahmed, H. Alanazi, and A. L. Marouf, "Modeling and optimization of the mechanical properties of date fiber reinforced concrete

containing silica fume using response surface methodology," *Case Studies in Construction Materials*, vol. 17, p. 1633, 2022.

[34] Z. Wan, T. He, N. Chang, R. Yang, and H. Qiu, "Effect of silica fume on shrinkage of cement-based materials mixed with alkali accelerator and alkali-free accelerator," *Journal of Materials Research and Technology*, vol. 22, pp. 825–837, 2023.

[35] Z. Li and L. Zhang, "Fly ash-based geopolymer with kappa-carrageenan biopolymer," *Biopolymers and Biotech Admixtures for Eco-Efficient Construction Materials*, pp. 173–192, 2016.